Cell Reports, Volume *16*

Supplemental Information

Transcription Factor NFIB Is a Driver of Small Cell Lung Cancer Progression in Mice and Marks Metastatic Disease in Patients

Ekaterina A. Semenova, Min-chul Kwon, Kim Monkhorst, Ji-Ying Song, Rajith Bhaskaran, Oscar Krijgsman, Thomas Kuilman, Dennis Peters, Wieneke A. Buikhuisen, Egbert F. Smit, Colin Pritchard, Miranda Cozijnsen, Jan van der Vliet, John Zevenhoven, Jan-Paul Lambooij, Natalie Proost, Erwin van Montfort, Arno Velds, Ivo J. Huijbers, and Anton Berns

Figure S1. Related to Figure 1. New mouse models for SCLC based on overexpression of two *Nfib* transcript variants

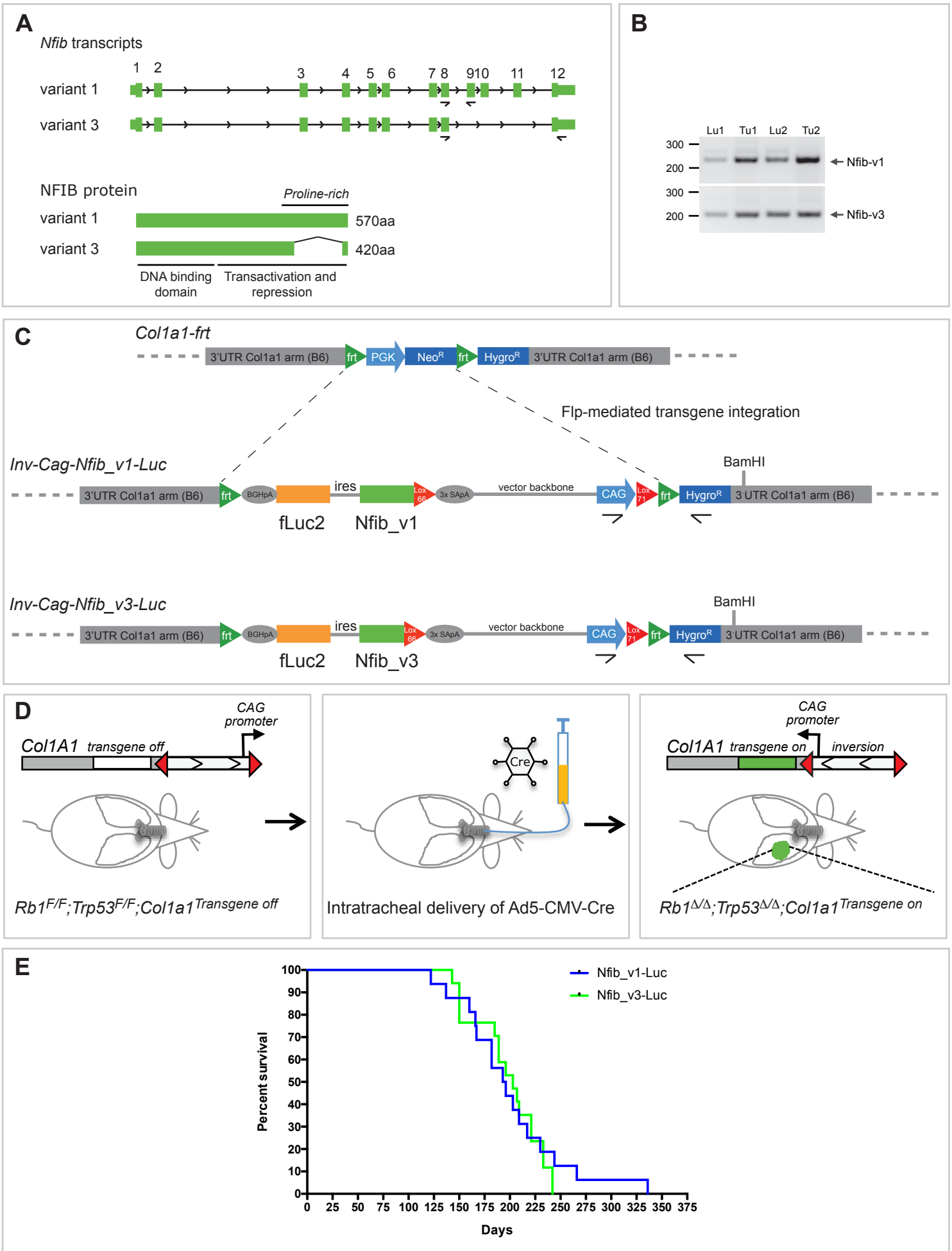

Figure S2. Related to Figure 1. Initial stages of tumor progression

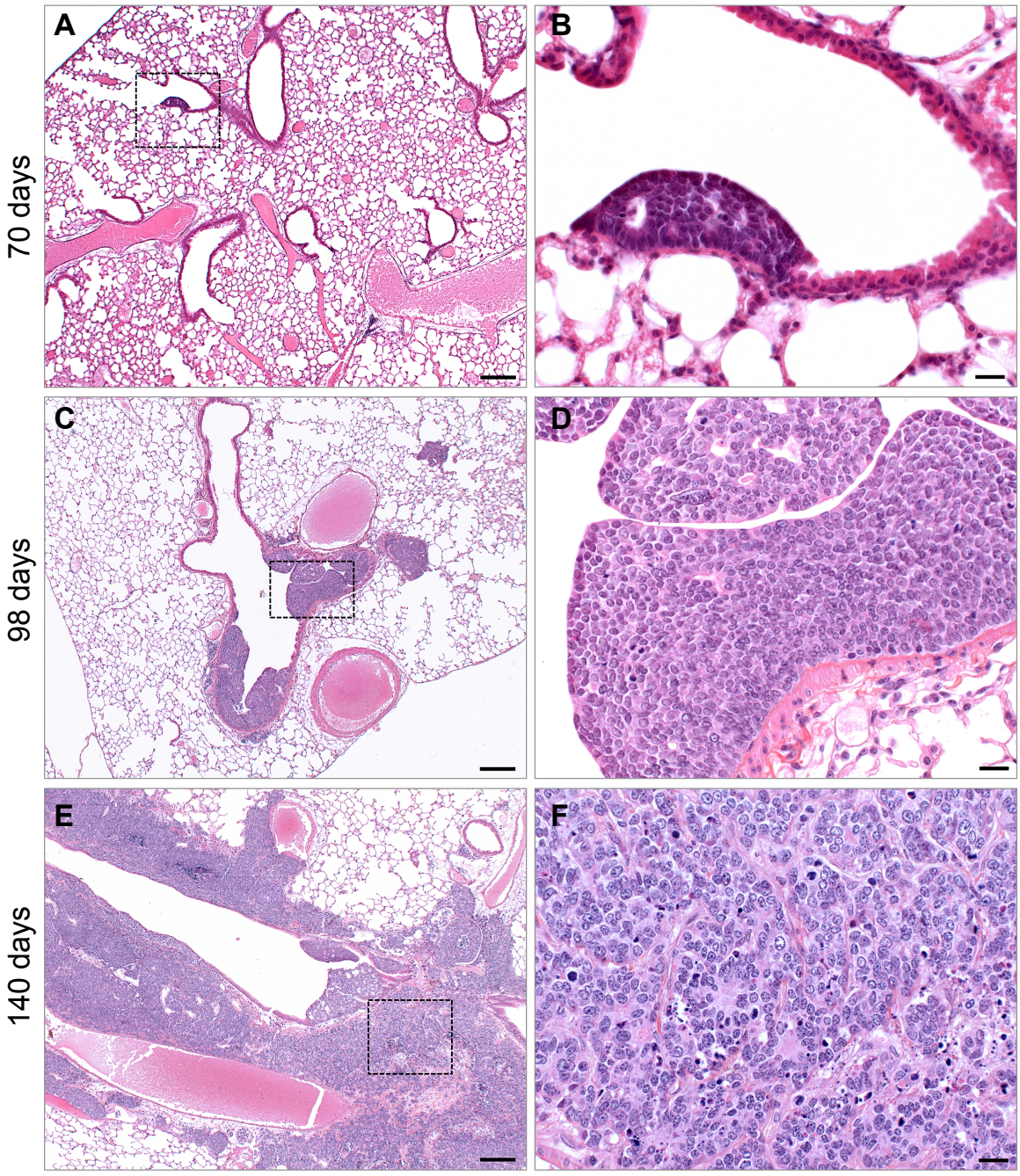

Figure S3. Related to Figure 1. Upper airway lesions in Nfib/Mycl cohort

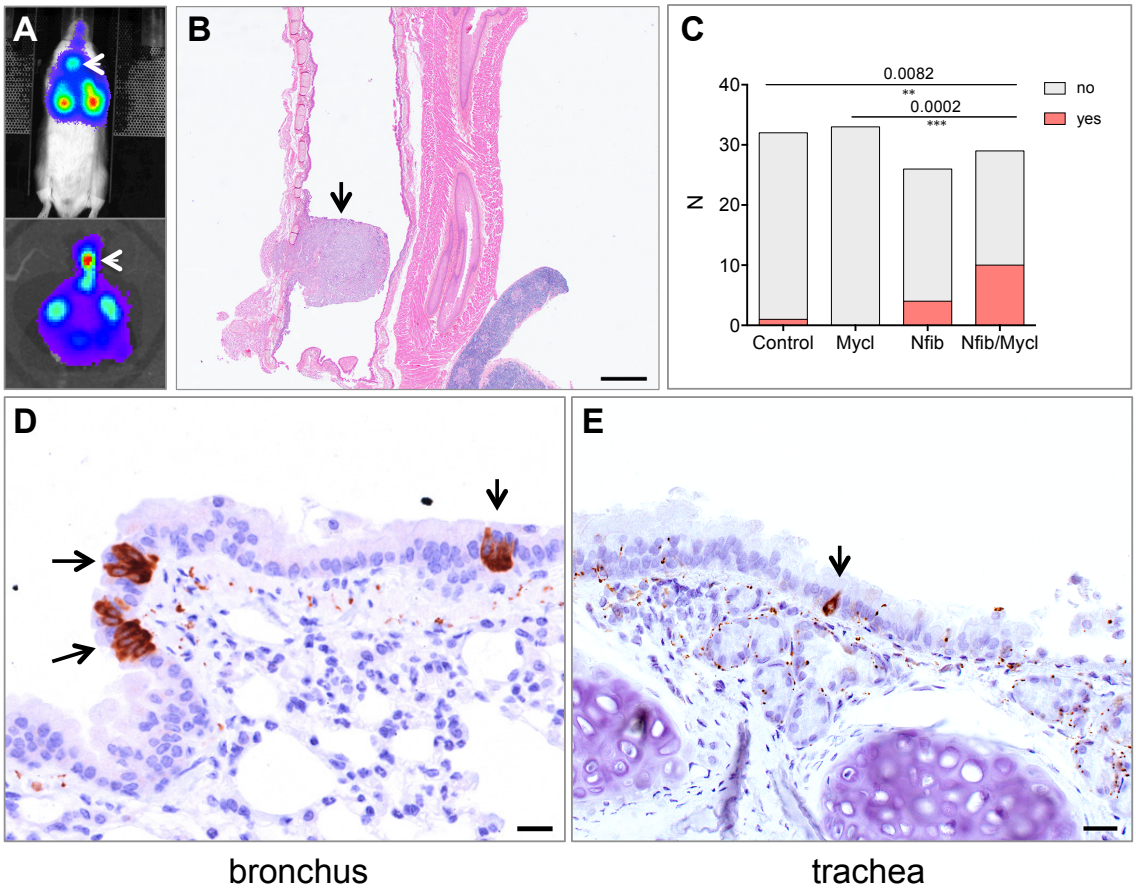

Figure S4. Related to Figure 3. NFIB promotes metastases and changes the metastatic profile

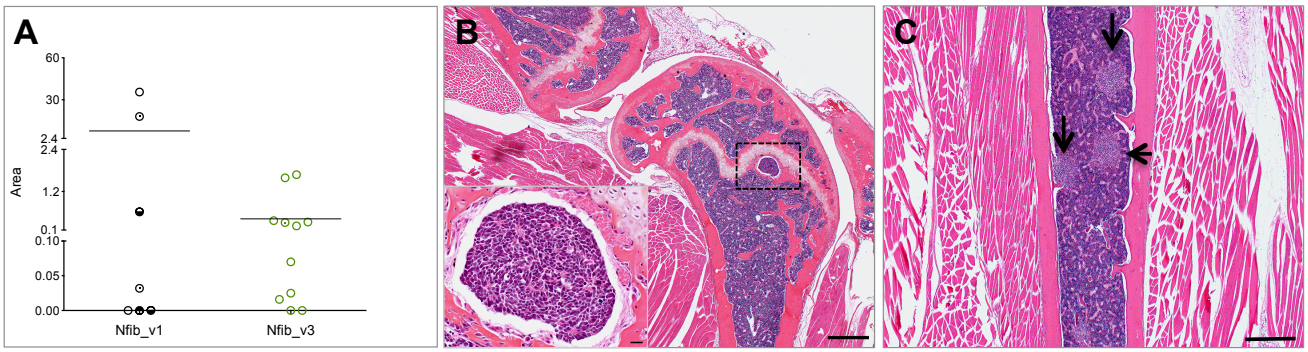

Figure S5. Related to Figure 4. Overexpression of mouse NFIB and the expression of putative NFIB target genes

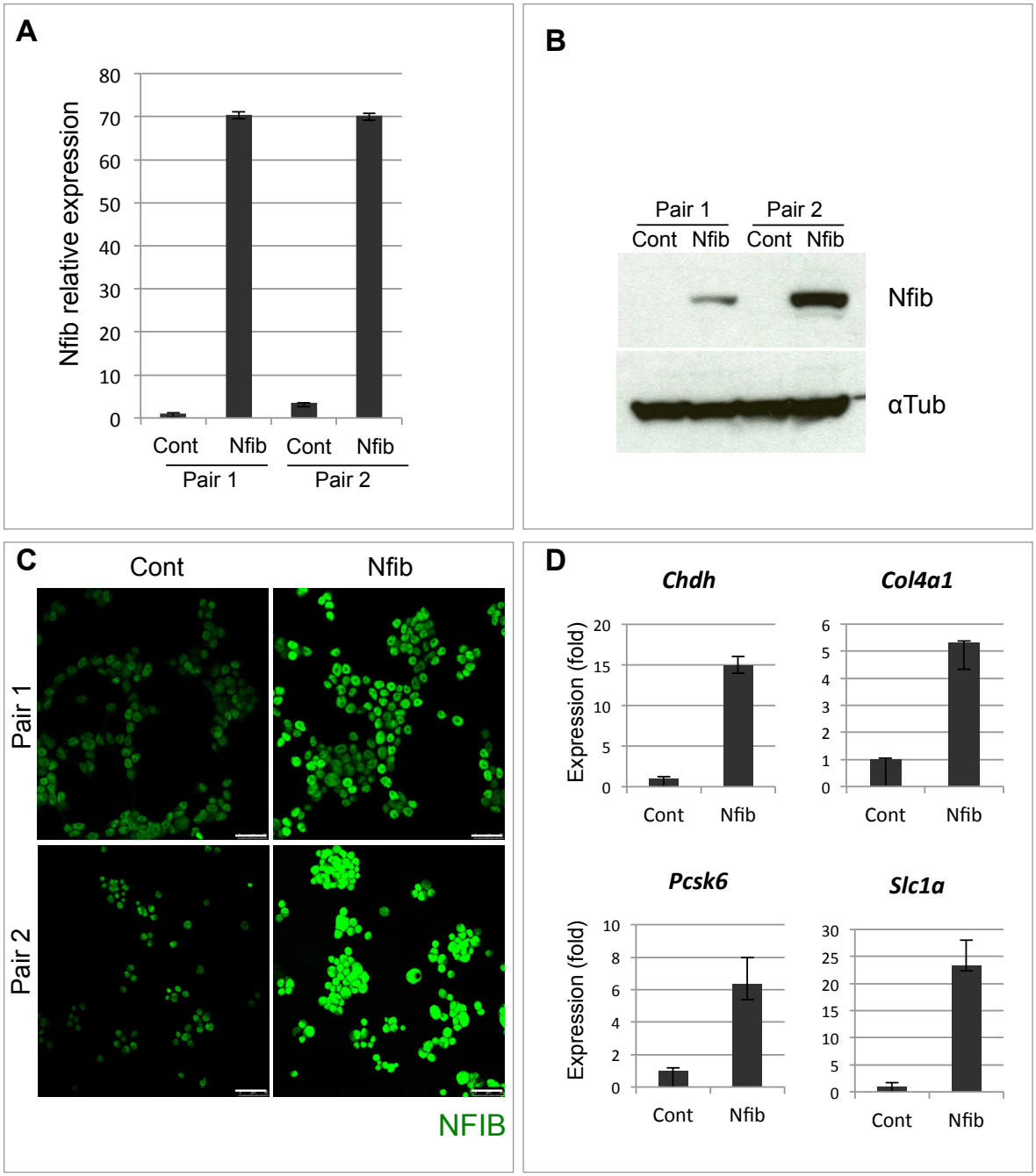

Figure S6. Related to Figure 5. NFIB drives tumor dedifferentiation and invasion

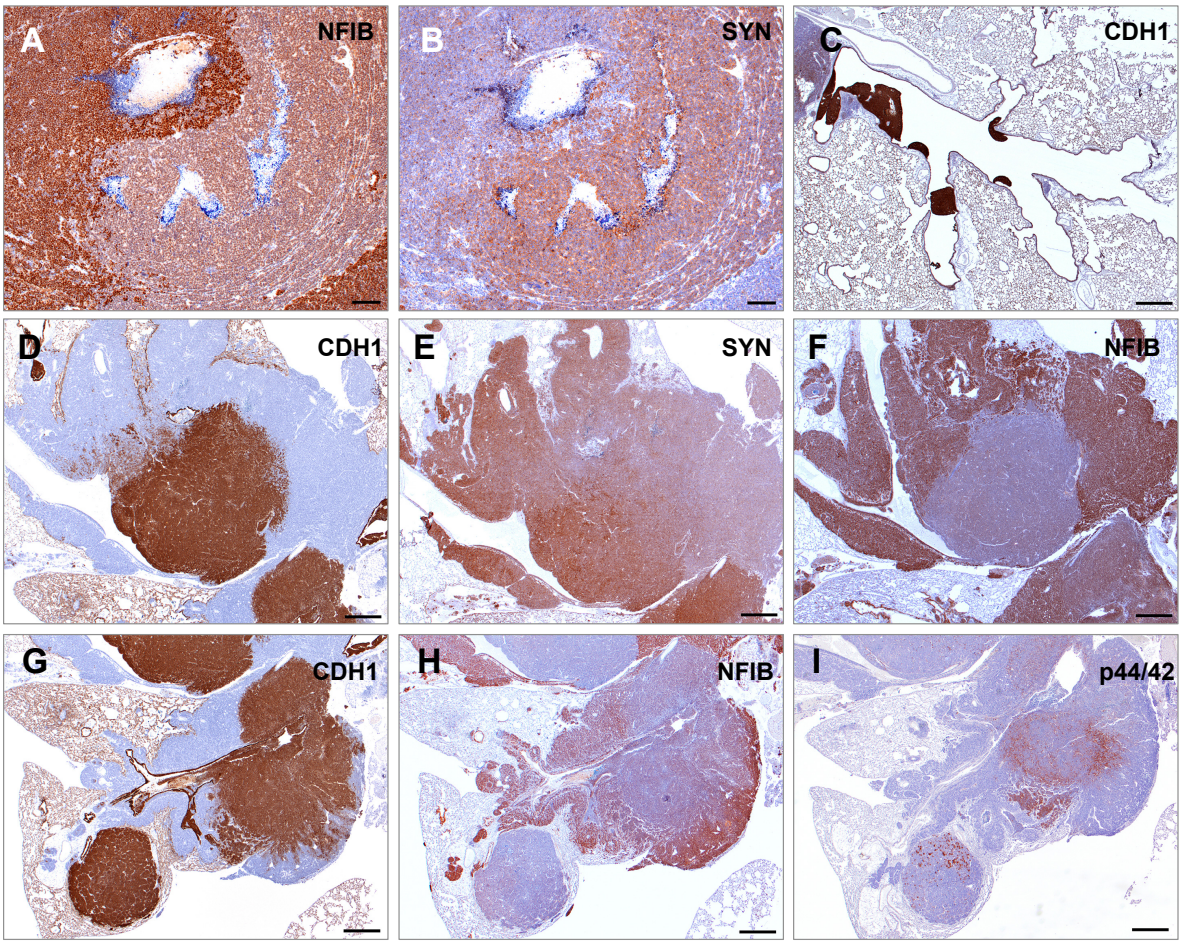

Figure S7. Related to Figure 5. NFIB drives tumor dedifferentiation and invasion (vascular invasion)

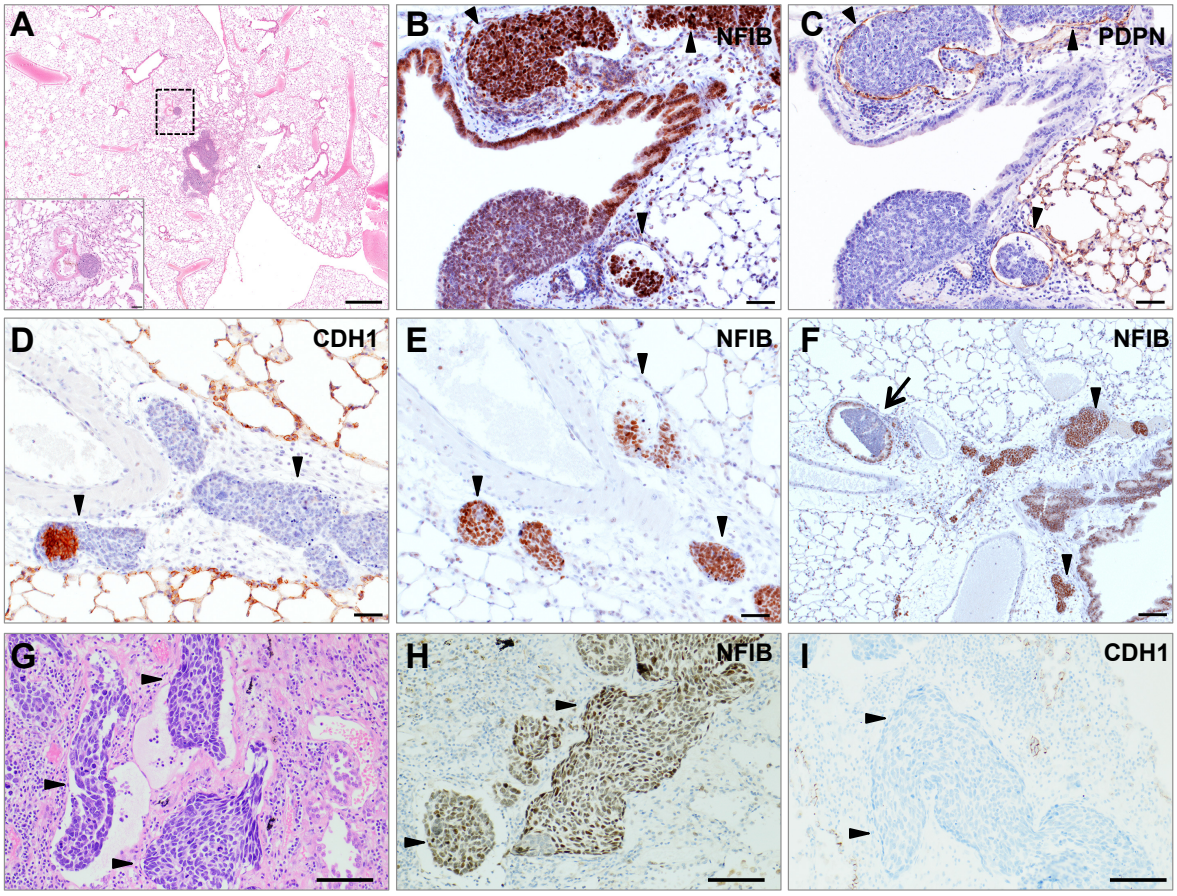

Figure S1. Related to Figure 1. New mouse models for SCLC based on overexpression of two *Nfib* transcript variants.
(A) Schematic representation of mouse *Nfib* transcripts and corresponding proteins. The Nfib protein from transcript variant 3 lacks the major part of a putative proline-rich transactivation domain at the C-terminus of the protein. Primers for RT-PCR analysis are indicated beneath exons 8, 9 and 12. (B) Detection of Nfib transcript variants 1 and 3 in normal mouse lung and in SCLC tumors for $Rb1^{F/F};Trp53^{F/F}$ mice with primers indicated in (A). Nfib_v1 gives a 234 bp product and Nfib_v3 a 210 bp. (C) Introduction of plasmids, *frt-invCag-Nfib_v1-Luc* or *frt-invCag-Nfib_v3-Luc*, in the *Col1a1-frt* construct in the *Col1a1* locus of the $Rb1^{F/F};Trp53^{F/F}$ embryonic stem cells (ESCs). ESCs were co-transfected with an *Nfib* coding inversion plasmid and a Flp-recombinase expression cassette. Clones were selected based on Hygromycin resistance. Correct Flp-mediated transgene integration was verified by a screening PCR with a forward primer in the CAG promoter and a reverse primer in the Hygromycin resistance gene. (D) Schematic representation of tumor induction. Mice with the $Rb1^{F/F};Trp53^{F/F};Col1a1^{Transgene}$ are intratracheally injected with an adeno-virus expressing Cre recombinase from the CMV promoter (Ad5-CMV-Cre). The virus infects lung epithelium, including neuro-endocrine cells. Cre recombinase deletes tumor suppressors *Rb1* and *Trp53*, and inverts the transgene between the two mutant loxP sites, i.e. Lox66-Lox71, leading to expression of the transgene, in this case the *Nfib* and the *Luciferase 2* gene. (E) Survival curve of two cohorts of Nfib mice, i.e. *InvCag-Nfib_v1-Luc;*$Rb1^{F/F};Trp53^{F/F}$ and *InvCag-Nfib_v3-Luc;*$Rb1^{F/F};Trp53^{F/F}$, following intratracheal injection with Ad5-CMV-Cre.

Figure S2. Related to Figure 1. Stages of tumor progression (Nfib/Mycl cohort)
(A) Representative HE of lung sections taken at 70 days following viral induction. (B) Magnification of the region in (A) indicated with the dotted line. (C) Representative HE of lung sections taken at 98 days following viral induction. (D) Magnification of the region in (C) indicated with the dotted line. (E) Representative HE of lung sections taken at 140 days following viral induction. (F) Magnification of the region in (E) indicated with the dotted line.
Scale bars in A, C, E represent 200 μm. Scale bars in B, D, F represent 20 μm.

Figure S3. Related to Figure 1. Upper airway lesions in Nfib/Mycl cohort
(A) Localized luciferase signal within the trachea (arrow). (B) Histological section of trachea with NE lesion (arrow). (C) Quantification of the number of animals with tracheal lesion within each cohort. (D) Section of bronchial epithelium of a normal lung (synaptophysin). (E) Section of the normal trachea (synaptophysin). Scale bar in B represents 500 μm. Scale bars in D and E represent 20 μm.

Figure S4. Related to Figure 3. NFIB promotes metastases and changes the metastatic profile. (A) Quantification of the percent area of liver samples covered by metastatic lesions in two transcript variant groups within Nfib cohort (Nfib_v1 and Nfib_v3). Circles with shaded upper half and shaded lower half indicate animals with kidney and bone metastasis, respectively. Circles marked with a central dot indicate animals with metastasis to both kidney and bone. (B and C) Metastasis within the bone and the bone marrow, respectively.

Figure S5. **Related to Figure 4. Overexpression of mouse NFIB and the expression of putative NFIB target genes**. The expression of exogenously overexpressed mouse *Nfib* was examined by qPCR (A) and western blot (B). (C) *Nfib* overexpression and cellular localization was examined by immunostaining. Scale bar represents 25 μm and 50 μm for Pair 1 and 2, respectively. (D) The expression of putative NFIB target genes was validated by qPCR. Error bars represent mean ± SD.

Figure S6. Related to Figure 5. NFIB drives tumor dedifferentiation. (A and B) Tumor stained with NFIB and SYN, respectively (Control cohort). (C) Early lesions stained with CDH1 (Mycl cohort). (D-F) Tumor stained with CDH1, SYN and NFIB, respectively (Control cohort). (G-I)) Tumor stained with CDH1, NFIB and p44/42, respectively (Control cohort). Scale bars in (A-B) represent 100 μm. Scale bars in (C-I) represent and 500 μm.

Figure S7. Related to Figure 5. NFIB drives tumor dedifferentiation and invasion. (A) Lung from an animal taken 98 days following tumor induction (HE). (B and C) NFIB and Podoplanin (PDPN) staining indicating localization of NFIB positive cells in lymph vessels (arrowheads). (D) CDH1 staining of NE cells within lymph vessels (arrowheads). (E and F) NFIB staining of NE cells within lymph vessels and within extravascular/extrabronchial space (arrowheads). Early NFIB negative lesion is indicated with an arrow (Mycl cohort) (G-I) Lymphangiovascular invasion (LVI) within human

LCNEC tumor sample, HE, NFIB and CDH1, respectively. Scale bar in (A) represents 500 μm, in (B-E) 50 μm, in (F-I) 100 μm.

Table S1. Related to Figure 4. Commonly upregulated and downregulated genes following NFIB overexpression

Table S2. Related to Figure 6. Patient data and scoring of FFPE immunohistochemical preparations

Supplemental Experimental Procedures

Nfib inversion constructs

Two transcript variants of murine *Nfib* were cloned in the *pFrt-invCAG-ires-Luc* vector (Addgene, cat. no. 63576). Variant 1 was the full-length transcript of *Nfib* and variant 3 lacked the last three exons, 9 to 11 (Figure S1A). The *pFrt-invCAG-Nfib_v1-Luc* and *pFrt-invCAG-Nfib_v3-Luc* vectors contain the chicken β–actin (CAG) promoter followed by a lox71 site, an ATG-coding Frt site, a firefly Luciferase2 (*Luc*) gene with polyadenylation site in the opposite orientation, an internal ribosomal entry sequence (ires) sequence, the *Nfib* cDNA, and a lox66 site followed by three modules of splice acceptor:polyadenylation site also all in the opposite orientation of the promoter sequence (Figure S1C). After Flp-mediated integration of these vectors in the *Col1a1* locus they act as inversion transgenes that display conditional expression of the *Nifb* and *Luciferase* after Cre recombination (Figure S1D).

Genetic engineering in $Rb1^{F/F};Trp53^{F/F}$ ESCs and generation of mice

The ESC clone was co-transfected with three plasmids: one expressing Flp^e (pCAGGS-Flp^e, Open Biosystems, cat. no. MES4488), one expressing GFP (pCAG-GFP, Addgene, cat. no. 11150) and either one of the Flp-in vectors, i.e. *pFrt-invCAG-Nfib_v1-Luc* or *pFrt-invCAG-Nfib_v3-Luc*. Transfection efficiency was evaluated the next day by monitoring for green fluorescence. After 24 hours, Hygromycin-B (Gibo-Invitrogen, cat. no. 10687-010) was added and medium was refreshed every other day. Clones were picked after 14 days and screened for correct integration of the inversion construct by a PCR with a forward primer located in the CAG promoter, 5'-CTGCATCAGGTCGGAGACGCTGTCG-3' and the reverse primer in the Hygromycin-B gene, 5'-GGGTTCGGCTTCTGGCGTGTGACC-3'. Product size was 319 bp. Three clones were used to generate chimeric mice: 349_reESC_Nfib_v1 clone 1 and clone 4, and 349_reESC_Nfib_v3 clone 1. Chimeric mice from clone 1 of the Nfib_v1 and clone 1 of Nifb_v3 were used to establish a line by crossbreeding to $Rb1^{F/F};Trp53^{F/F}$ mice.

Experimental cohorts

$Rb1^{F/F};Trp53^{F/F}$ (Control cohort), *invCAG-Luc;*$Rb1^{F/F};Trp53^{F/F}$ (Control cohort), *invCAG-Mycl-Luc;*$Rb1^{F/F};Trp53^{F/F}$ (Mycl cohort) mice have been described earlier (Huijbers et al., 2014; Meuwissen et al., 2003). The latter two genotypes also contain an inversion construct in the *Col1a1* locus, one containing only the *Luc* gene and the other the *Mycl* gene, an ires sequence and the *Luc* gene, respectively. The Nfib cohort contains both *invCAG-Nfib_v1-Luc;*$Rb1^{F/F};Trp53^{F/F}$ *and invCAG-Nfib_v3-Luc;*$Rb1^{F/F};Trp53^{F/F}$ mice. The two Nfib genotypes were analyzed independently but merged, since no difference was observed between the two genotypes in survival and metatstasis. The Nfib/Mycl cohort was obtained by crossbreeding *invCAG-Nfib_v1-Luc;*$Rb1^{F/F};Trp53^{F/F}$ (from 349_reESC_Nfib_v1 clone 1) with *Mycl-Luc;*$Rb1^{F/F};Trp53^{F/F}$ mice. In the Nfib, Mycl and Control (Luc) cohorts, chimeric mice obtained after ESC injection were included in the experimental groups. The $Rb1^{F/F};Trp53^{F/F}$ mice in the Control cohort were littermate controls obtained by crossbreeding to either Nfib or Mycl Cohort mice. The various inversion transgenes were maintained heterozygous in all cohorts, though in the Nfib/Mycl cohort two different transgenes were present in the *Col1a1* locus.

Ethics statement

Mice were housed under standard conditions of feeding, light and temperature with free access to food and water. Male and female mice were represented equally in the experimental cohorts.

Tumor induction via intratracheal Ad5-CMV-Cre virus administration

Mice from the different cohorts were treated with cyclosporine A (Novartis) orally in the drinking water, 1 week prior to adenovirus administration and 2-3 weeks following infection. Viral Ad5-CMV-Cre particles (20 µl, 1 x 10^9; Gene Transfer Vector Core, University of Iowa) were injected intratracheally. Mice were monitored daily for signs of illness and culled upon respiratory distress or excessive weight loss (>20% of initial weight). A small number of experimental mice were culled at defined time points; 10, 14 and 20 weeks post viral infection.

Imaging of tumors

In vivo bioluminescence imaging was performed and quantified as described by Hsieh C. et al. 2005 (Hsieh et al., 2005) on a cryogenically cooled IVIS system (Xenogen Corp., CA, USA) using LivingImaging acquisition and analysis software (Xenogen). Luciferase units are photons/second x cm^2 x sr.

Histology, Immunohistochemistry, and Quantification

Tissues and organs were collected and fixed in EAF fixative (ethanol/acetic acid/formaldehyde/ saline at 40:5:10:45 v/v) and embedded in paraffin. Sections were prepared at 2 μm thickness from the paraffin blocks and stained with hematoxylin and eosin (HE) according to standard procedures. For immunohistochemistry (IHC), 4 um-thick sections were made on which antibodies were applied such as: Synaptophysin (Abcam, ab32127), NCAM (Chemicon, AB5032), CDH1 (Cell signaling, #3195), NFIB (Thermo Scientific, PA5-28299), CGRP (Sigma, C8198), Phospho-p44/42 (Cell Signaling, #4370). The sections were reviewed with a Zeiss Axioskop2 Plus microscope (Carl Zeiss Microscopy, Jena, Germany) and images were captured with a Zeiss AxioCam HRc digital camera and processed with AxioVision 4 software (both from Carl Zeiss Vision, München, Germany). For the quantification of liver metastasis, NCAM staining liver sections were analyzed using ImageJ software (National Institutes of Health).

Copy number analysis and qPCR analysis

Genomic DNA and total cellular RNA were simultaneously isolated from snap frozen tumor sample or normal lung tissue using the Allprep DNA/RNA/Protein mini kit (Qiagen) according to the manufacturer's instructions. Tissues were homogenized in RLT buffer using TissueLyser (Qiagen). The genomic DNA copy numbers for *Nfib* and *Mycl* were determined by using pre-designed Taqman copy number assays (Applied Biosystems). The probes of *Nfib* (Mm00128854_cn) and *Mycl* (Mm00558489_cn) were labeled with FAM and the Taqman copy number reference assay, mouse *Tert* (part #4458368) and mouse *Tfrc* (part #4458366) labeled with VIC were used for the internal reference copy number. Genomic DNA from normal lung tissue and mouse embryonic stem cells were used as normal controls. The cDNA equivalent to total RNA from same tumor sample was prepared using the Superscript II reverse transcriptase (Invitrogen) according to manufacturer's instructions. For real-time PCR, cDNA was subjected to 40 cycles of amplification using Taqman gene expression assays (Nfib, Mm01257775_m1 and Mm00616076_s1, Mycl, Mm00493155_m1) labeled with FAM and the pre-developed Taqman assay reagents of mouse beta actin (part #4352341) was used for normalization. For the validation of RNAseq gene expression analysis, total RNA from SCLC cells was extracted using RNeasy Mini Kit (Qiagen) and cDNA was prepared in same procedure as that for tumor samples. For real-time PCR, SYBR Green expression assay (Applied Biosystems) was performed with following primers (mouse Actin, 5'- aaatcgtgcgtgacatcaaa-3' and 5'-aaggaaggctggaaaagagg-3'; mouse Agt, 5'-tcaacacctacgttcacttcca-3' and 5'- gatcatgggcacagacacc-3'; mouse Chdh, 5'- cactgccttctcggctct-3' and 5'-tcctctatccaccgacagga-3'; mouse Clu, 5'-gatccaccaggctcaacag-3' and 5'-tgcggtcatcttcaccttc-3'; mouse Col4a1 5'-cgggagagaaaggtgctgt -3' and 5'- ctccaggcaagccatcaa -3'; mouse Itga 5'- atcctcctgagcgccttt -3' and 5'-tttcttctttagtggccttttga -3'; mouse Kcnma 5'- gtacctgtggaccgtttgct -3' and 5'- caccacctcctcttttttcgt -3'; mouse Pcsk6 5'-gactccagaagacgaggaagag -3' and 5'- acactcgggatggcacac -3'; mouse Ror1 5'-tgcaggggggaaatagaaaatc-3' and 5'-atggcgaactgagagcactt-3'; mouse Slc1a2 5'- gacgggatgaacgtcttaggt-3' and 5'- accatcagcttggcctgt-3'; mouse Sparc 5'-agaggaaacggtcgaggag-3' and 5'-ctcacacaccttgccatgtt-3' as per the manufacturer's instructions. The data from mouse Actin was used as normalization control.

***Nfib* splicing variants**

The cDNA from normal lung and tumor was used to examine the expression of full length *Nfib* (transcript variant 1) and *Nfib* transcript variant 3 lacking exon 9-11. To detect the full length *Nfib*, PCR primers designed from the *Nfib* exon 8 (mNfib_E8; 5'-tcaactcgaactccacctcc-3') to *Nfib* exon9 (mNfib_E9; 5'-gacaggtgtgaaatggccag-3') were used and the size of full length *Nfib* PCR product is 234bp. For the *Nfib* transcript variant 3, PCR primers designed from *Nfib* exon 8 (mNfib_E8) to exon 12 (mNfib_E12; 5'-aaaggaaccaagctagccca-3') of *Nfib* full length cDNA were used and the size of *Nfib* transcript variant 3 PCR product is 210bp. Phusion high fidelity PCR kit (New England Biolabs) was used for the amplification of *Nfib* splicing variants following the manufacturer's instructions.

DNA sequencing and Copy number profiling

The amount of double stranded DNA in genomic DNA samples was quantified using the Qubit® dsDNA HS Assay Kit (Invitrogen). Up to 250 ng of double stranded genomic DNA was fragmented by Covaris shearing to obtain fragment sizes of 160–180 bp. Samples were purified with the Agencourt AMPure XP PCR Purification beads according to manufacturer's instructions (Beckman Coulter, cat no A63881). DNA library preparation for Illumina sequencing was done with the TruSeq® DNA LT Sample Preparation kit (Illumina). The double-stranded DNA input amount was lower than advised by the Truseq protocol, so we used up to 250 ng of double-stranded DNA, such that 2.5 times less adapter concentration was used than prescribed in the TruSeq protocol. During enrichment PCR, 10 cycles were necessary to obtain enough yield for sequencing. All DNA libraries were analyzed on a BioAnalyzer system (Agilent Technologies) using the DNA7500 chips for determining the molarity. Up to ten

uniquely indexed samples were pooled equimolarly to give a final concentration of 10 nM. Pools were then sequenced using an Illumina HiSeq2000/2500 machine to coverage of 0.5×. This was done in one lane of a single-end 51 bp run according to manufacturer's instructions.
Reads were aligned to the reference genome (mm10) using the Burrows-Wheeler Aligner (BWA 7.10) (Li and Durbin, 2009). To obtain copy number profiles we use CopywriteR tool (Kuilman et al., 2015). The CopywriteR program was adapted for low coverage sequencing without peak calling algorithm. A depth-of-coverage method was used for 20-kb bins, and the read count was normalized for GC content and mappability. Log2-transformed ratios were calculated for all tumor samples versus reference (tail) sample. The normalized and corrected profiles were further analysed by circular binary segmentation (CBS) (Olshen et al., 2004). DNA copy number was visualized using the Broad Institute's Integrated Genome Viewer (http:// www.broadinstitute.org/igv).
Next-generation MPS Mate-pair libraries were prepared using the Nextera Mate Pair Sample Preparation Kit (Illumina, San Diego, CA, USA). Paired-end adapters were ligated to the fragments and the library was amplified by 18 cycles of PCR. Mate-pair libraries were subjected to 2 x 51 bases PES on a HiSeq 2000 (Illumina), following the manufacturers protocol. After adapter trimming the reads were aligned to the mm10 reference genome using BWA-MEM (version 0.7.5, http://arxiv.org/abs/1303.3997) (Stephens et al., 2011). Intrachromosomal rearrangements were detected by extracting paired reads that have a mapping quality > 50 for both ends and connect two locations that are at least 50kb apart. If two or more of those distinct read pairs are found within 30kb on both ends, the rearrangement is recorded.

Overexpression of NFIB in mouse SCLC cells
Cell lines from *invCAG-Mycl-Luc;Rb1$^{F/F}$;Trp53$^{F/F}$* (Mycl cohort) SCLC tumors were derived as previously described (Calbo et al., 2011). Cells were maintained in modified HITES medium DMEM/F12 (1:1) (GIBCO) supplemented with 4µg/ml Hydrocortisone (Sigma), 5 ng/ml murine EGF (Invitrogen), Insulin-Transferrin-Selenium mix/solution (GIBCO) and 10% Fetal Bovine Serum (GIBCO). For overexpression of NFIB, Myc-tagged ORF clone of mouse NFIB from Origene (MR206682) was excised and cloned into the pMSCV-puro retroviral vector (Invitrogen). Puromycin was used to select NFIB overexpressing cells. NFIB expression was validated by western blot and immunocytochemistry using antibody against NFIB (Thermo Scientific, PA5-28299) performed by standard procedures.

RNA-seq analysis
After quality filtering according to the illumina pipeline, 51-bp single-end reads were mapped to the mouse genome (mm10), using TopHat (2.0.12) (Trapnell et al., 2009). TopHat was run with default. Reads with mapping quality less than 10 and non-primary alignments were discarded. Remaining reads were counted using HTSeq-cout (Anders et al., 2015). Statistical analysis of the differential expression of genes was performed using DESeq2 (Love et al., 2014). Normalized read counts from DESeq2 are used to calculate the average fold change between each pairs (Table S1). Biological network analysis was performed using Ingenuity Pathway Analysis (IPA) (v 9.0, Ingenuity Systems, Mountain View, CA, USA) to predict potential biological processes, pathways and molecules affected by DEGs.

Human SCLC patient specimens
This study was approved by institutional review board of the NKI-AVL. We collected archived FFPE samples of 48 TC, AC, LCNEC and SCLC patients. The FFPE TC, AC, LCNEC and SCLC samples were primary and metastatic tumors diagnosed as stage I–IV tumors. All tumor samples were reviewed by at least two independent expert pathologists. The diagnosis was histomorphologically confirmed by H&E staining and immunohistochemistry.
Immunohistochemistry of the FFPE tumor samples was performed on a BenchMark Ultra autostainer (E-Cadherin) or Discovery Ultra autostainer(NFIB). Briefly, paraffin sections were cut at 3 µm, heated at 75°C for 28 minutes and deparaffinized in the instrument with EZ prep solution (Ventana Medical Systems). Heat-induced antigen retrieval was carried out using Cell Conditioning 1 (CC1, Ventana Medical Systems) for 32 minutes at 95^{0}C. E-cadherin was detected using NCH-38 (1/200 dilution, 32 minutes at 37^{0}C, Dako), NFIB was detected using a polyclonal antibody (Cat.No PA5-28299) (1/100 dilution, 32 minutes at 37^{0}C, ThermoScientific). E-Cadherin bound antibody was visualized using the Optiview Amplification kit (Ventana Medical Systems). Followed by the Optiview DAB detection kit (Ventana Medical systems). NFIB bound antibody was visualized using Anti-Rabbit HQ (Ventana Medical systems) for 12 minutes at 37^{0}C followed by Anti-HQ HRP (Ventana Medical systems) for 12 minutes at 37^{0}C, followed by the ChromoMap DAB detection kit (Ventana Medical Systems). Slides were counterstained with Hematoxylin II and Bluing Reagent (Ventana Medical Systems).

The H-score was determined by assessing the extent of nuclear immunoreactivity for NFIB and ECAD by KM and ES (Table S2). The score is obtained by the formula: 3 x percentage of strongly staining nuclei + 2 x percentage of moderately staining nuclei + percentage of weakly staining nuclei, giving a range of 0 to 300.
An experienced pathologist and KM scored the positive Mib-1 fraction by assessing the area with the highest positive fraction in the tumor. At 40X magnification the positive fraction was estimated by comparison to pictures with predefined positive fractions.
Overall survival was analyzed with the study cohort of 48 TC, AC, LCNEC and SCLC patients considering age of diagnosis, gender, tumor stage, treatment, smoking history and overall survival. This data was obtained by reviewing the electronic patients files of the NKI-AVL. If data was not available other hospitals were contacted for missing data (Table S2). The median follow-up time for this cohort of 48 TC, AC, LCNEC and SCLC patients was 38 months, and 42% of the patients were alive at the time of last follow-up.

Supplemental References

Anders, S., Pyl, P. T., and Huber, W. (2015). HTSeq--a Python framework to work with high-throughput sequencing data. Bioinformatics *31*, 166-169.
Calbo, J., van Montfort, E., Proost, N., van Drunen, E., Beverloo, H. B., Meuwissen, R., and Berns, A. (2011). A functional role for tumor cell heterogeneity in a mouse model of small cell lung cancer. Cancer cell *19*, 244-256.
Hsieh, C. L., Xie, Z., Liu, Z. Y., Green, J. E., Martin, W. D., Datta, M. W., Yeung, F., Pan, D., and Chung, L. W. (2005). A luciferase transgenic mouse model: visualization of prostate development and its androgen responsiveness in live animals. J Mol Endocrinol *35*, 293-304.
Huijbers, I. J., Bin Ali, R., Pritchard, C., Cozijnsen, M., Kwon, M. C., Proost, N., Song, J. Y., de Vries, H., Badhai, J., Sutherland, K.*, et al.* (2014). Rapid target gene validation in complex cancer mouse models using re-derived embryonic stem cells. EMBO molecular medicine *6*, 212-225.
Kuilman, T., Velds, A., Kemper, K., Ranzani, M., Bombardelli, L., Hoogstraat, M., Nevedomskaya, E., Xu, G., de Ruiter, J., Lolkema, M. P.*, et al.* (2015). CopywriteR: DNA copy number detection from off-target sequence data. Genome biology *16*, 49.
Li, H., and Durbin, R. (2009). Fast and accurate short read alignment with Burrows-Wheeler transform. Bioinformatics *25*, 1754-1760.
Love, M. I., Huber, W., and Anders, S. (2014). Moderated estimation of fold change and dispersion for RNA-seq data with DESeq2. Genome biology *15*, 550.
Meuwissen, R., Linn, S. C., Linnoila, R. I., Zevenhoven, J., Mooi, W. J., and Berns, A. (2003). Induction of small cell lung cancer by somatic inactivation of both Trp53 and Rb1 in a conditional mouse model. Cancer cell *4*, 181-189.
Olshen, A. B., Venkatraman, E. S., Lucito, R., and Wigler, M. (2004). Circular binary segmentation for the analysis of array-based DNA copy number data. Biostatistics *5*, 557-572.
Stephens, P. J., Greenman, C. D., Fu, B., Yang, F., Bignell, G. R., Mudie, L. J., Pleasance, E. D., Lau, K. W., Beare, D., Stebbings, L. A.*, et al.* (2011). Massive genomic rearrangement acquired in a single catastrophic event during cancer development. Cell *144*, 27-40.
Trapnell, C., Pachter, L., and Salzberg, S. L. (2009). TopHat: discovering splice junctions with RNA-Seq. Bioinformatics *25*, 1105-1111.